

Multi-objective optimization of friction stir welding parameters using desirability approach to join Al/SiC_p metal matrix composites

P. PERIYASAMY¹, B. MOHAN², V. BALASUBRAMANIAN³, S. RAJAKUMAR³, S. VENUGOPAL

1. Department of Mechanical Engineering, St. Peter's Engineering College, Avadi, Chennai 600 054, Tamil Nadu, India;

2. Department of Production Technology, MIT, Anna University, Chennai 600 044, Tamil Nadu, India;

3. Center for Materials Joining and Research (CEMAJOR), Department of Manufacturing Engineering, Annamalai University, Annamalainagar 608 002, Tamil Nadu, India;

4. IGCAR-Kalpakkam, Chennai, India

Received 7 March 2012; accepted 20 August 2012

Abstract: Silicon carbide particulate (SiC_p) reinforced cast aluminium (Al) based metal matrix composites (MMCs) have gained wide acceptance in the fabrication of light weight structures requiring high specific strength, high temperature capability and good wear resistance. Friction stir welding (FSW) process parameters play major role in deciding the performance of welded joints. The ultimate tensile strength, notch tensile strength and weld nugget hardness of friction stir butt welded joints of cast Al/SiC_p MMCs (AA6061 with 20% (volume fraction) of SiC_p) were investigated. The relationships between the FSW process parameters (rotational speed, welding speed and axial force) and the responses (ultimate tensile strength, notch tensile strength and weld nugget hardness) were established. The optimal welding parameters to maximize the mechanical properties were identified by using desirability approach. From this investigation, it is found that the joints fabricated with the tool rotational speed of 1370 r/min, welding speed of 88.9 mm/min, and axial force of 9.6 kN yield the maximum ultimate tensile strength, notch tensile strength and hardness of 265 MPa, 201 MPa and HV114, respectively.

Key words: metal matrix composites; friction stir welding; Al/SiC_p composites; microstructure

1 Introduction

Metal matrix composites (MMCs) are valued by the aerospace industry as potential futuristic materials due to the high specific strength. In 2010, the market share for MMCs grew to 4.9×10^6 kg increased 6.3% over the past five years [1]. However, the use of MMCs in industrial applications is limited by the difficulties associated with joining MMCs to themselves or other materials. Recently, a new solid state welding process popularly known as friction stir welding (FSW) has been used to weld MMCs.

Compared to many conventional fusion welding methods, the FSW process has the advantages such as good mechanical properties, low residual stress and distortion, and reduced occurrence of defects [2–3]. This welding technique, attracting an increasing amount of research interest, is applied to the aerospace, automotive, and shipbuilding industries. A thorough understanding of

FSW process and the consequent evaluation of weld mechanical properties are needed for production of components and structures. For this reason, detailed researches are required [4]. It is well known that whatever the welding method is the main challenge for the manufacturer is selecting the optimum welding parameters which would produce an excellent welded joint. To predict the optimum welding parameters accurately without consuming time, materials, and labor effort, various methods are available and one such method is response surface methodology (RSM).

VIJAYAN [5] reported the optimization of FSW process parameters for AA5083 aluminum alloy with multiple responses based on orthogonal array with gray relational analysis. He found the optimum levels of the process parameters to attain maximum tensile strength and minimum power consumption. SARSILMAZ [6] studied the effect of FSW parameters such as spindle rotational speed, traverse speed, and stirrer geometry on ultimate tensile strength (UTS) and hardness of welded

joints. In this work, the full-factorial experimental design was used to obtain the response measurements. Analysis of variance (ANOVA) and main effect plot were used to determine the significant parameters and set the optimal level for each parameter. A linear regression equation was also developed to predict each output characteristic.

TANSEL et al [7] adopted the genetically optimized neural network system (GONNS) to estimate the optimal operating condition of the FSW process. Five separate ANNs represented the relationship between two identical input parameters and each one of the considered characteristics of the welding zone. Genetic algorithm (GA) searched for the optimized parameters to make one of the parameters maximum or minimum, while the other four are kept within the desired range. RAJAKUMAR et al [8] proposed models using RSM to investigate the effect of FSW process parameters and weld parameters on the tensile strength of AA7075 aluminum alloy. In this work, an empirical relationship was developed relating FSW process parameters and tensile strength of the joints using statistical tools such as design of experiments, analysis of variance, and regression analysis. The developed empirical relationship can be effectively used to predict the tensile strength of FSW joints at the 95% confidence level. JAYARAMAN et al [9] developed an empirical relationship relating base metal properties of cast Al alloys and optimized FSW parameters. The developed relationships can be effectively used to predict the optimum FSW process parameters to fabricate defect-free joints with high tensile strength from the known base metal properties of cast aluminum alloys.

There have been a lot of efforts to understand the effect of process parameters on material flow behavior, microstructure formation, and mechanical properties of friction stir welded joints. Finding the most effective parameters of friction stir welding process as well as realizing their influence on joint properties have been major topics for researchers [10–13]. The optimization of the important parameters, such as axial pressure (F), tool rotational speed (N), and traverse speed (S), on joint properties has been investigated. The effects of process parameters on multi-responses such as tensile strength (TS), notch tensile strength (NTS) and weld nugget hardness (HV) are hitherto not reported. It is important to evaluate the mechanical properties of welded joint to describe its performance. Tensile strength and weld nugget hardness are the most vital mechanical properties of FSW joints. In this work, along with the tensile strength, notch tensile strength and weld nugget hardness were also considered to evaluate the performance of the FSW joints of cast AA6061/20%SiC_p MMCs. Therefore, the first aim is to employ RSM to develop empirical relationships relating the FSW process parameters (tool

rotational speed, welding speed and axial force) and the three output responses (i.e., tensile strength, notch tensile strength and weld nugget hardness). The second aim is to find the optimal welding combination that would maximize the tensile strength, notch tensile strength and the weld nugget hardness of the joints.

2 Methodology

2.1 Response surface methodology

Engineers often wish to determine the values of the input process parameters at which the responses reach their optimum. The optimum could be either a minimum or a maximum of a particular function in terms of the process input parameters. Response surface methodology (RSM) is a collection of mathematical and statistical technique useful for analyzing problems in which several independent variables influence a dependent variable or response and the goal is to optimize the response [14]. In many experimental conditions, it is possible to represent the independent factor in quantitative form as given in Eq. (1). Then, these factors can be thought to have a functional relationship or response as follows:

$$Y = \Phi(x_1, x_2, \dots, x_k) + e_r \quad (1)$$

Between the response Y and x_1, x_2, \dots, x_k of k quantitative factors, the function Φ is called response surface or response function. The residual e_r measures the experimental errors. For a given set of independent variables, a characteristic surface is responded. When the mathematical form of Φ is not known, it can be approximate satisfactorily within the experimental region by polynomial. In the present work, RSM was applied for developing the mathematical model in the form of multiple regression equations for the quality characteristic of the friction stir welded cast AA6061/20%SiC_p MMCs. In applying the response surface methodology, the independent variable is viewed as a surface to which a mathematical model is fitted.

Representing the tensile strength of the joint by Y , the response is a function of tool rotational speed (N), welding speed (S) and axial force (F), and it can be expressed as

$$Y = f(N, S, F)$$

The second order polynomial (regression) equation used to represent the response surface is given by [15]

$$Y = b_0 + \sum b_i x_i + \sum b_{ii} x_i^2 + \sum b_{ij} x_i x_j + e_r \quad (2)$$

2.2 Experimental design

The test was designed based on three-factor, five-level central composite rotatable design with half replication [14]. The friction stir-welding input variables are rotational speed, welding speed and axial force. In

order to find the range of each process parameter, trial weld runs were performed by changing one of the process parameters at a time. Absence of macro-level welding defects, smooth and uniform welded surface with the sound face were the criteria of selecting the feasible working range. Table 1 displays the macrographs to provide the evidence for fixing the feasible working range of welding parameters. Table 2 shows the process

variables, their coded and actual values. Statistical software Design-Expert V8 was used to code the variables and to establish the design matrix (shown in Table 3). RSM was applied to the experimental data using the same software, and polynomial Eq. (2) was fitted to the experimental data to obtain the regression equations for all responses. The statistical significance of the terms in each regression equation was examined

Table 1 Cross-sectional macrostructure of FSW joints fabricated outside feasible welding range

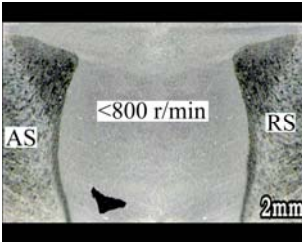
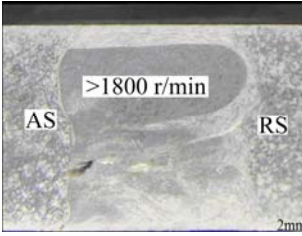
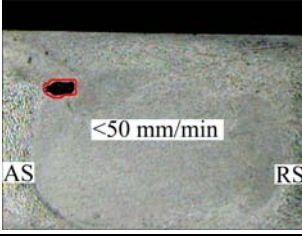
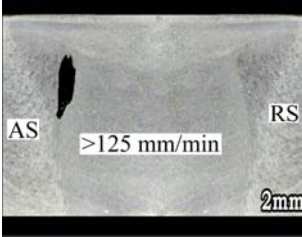
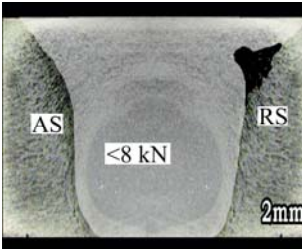
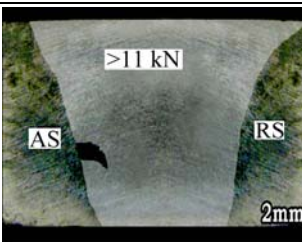
FSW parameter	Parameter range	Weld cross-section	Name of defect	Location of defect
Rotational speed	<800 r/min		Piping defect	Root region of weld nugget of advancing side
Rotational speed	>1800 r/min		Small pin hole	Middle of weld nugget of advancing side
Welding speed	<50 mm/min		Large pin hole	Shoulder influenced region of weld nugget of advancing side
Welding speed	>125 mm/min		Tunnel defect	Middle of weld nugget of advancing side
Axial force	<8 kN		Tunnel defect	Shoulder influenced region of weld nugget of retreating side
Axial force	>11 kN		Worm hole	Middle region of weld nugget of advancing side

Table 2 Important FSW process parameters and their feasible welding range

Factor	Factor level				
	-1.682	-1	0	+1	+1.682
Tool rotational speed, $N/(r \cdot \text{min}^{-1})$	800	1002	1300	1597	1800
Welding speed, $S/(\text{mm} \cdot \text{min}^{-1})$	50	65.2	87.5	109.8	125
Axial force, F/kN	8	8.61	9.5	10.39	11

Table 3 Experimental design matrix and results

Experiment No.	Rotational speed	Welding speed	Axial force	UTS of joint/MPa	NTS of joint/MPa	Weld nugget hardness (HV)
1	-1	-1	-1	182	170	90
2	1	-1	-1	210	181	93
3	-1	1	-1	181	177	96
4	1	1	-1	227	183	99
5	-1	-1	1	187	174	97
6	1	-1	1	215	185	101
7	-1	1	1	183	175	93
8	1	1	1	243	186	96
9	-1.682	0	0	180	172	93
10	1.682	0	0	246	188	99
11	0	-1.682	0	193	179	96
12	0	1.682	0	225	182	101
13	0	0	-1.682	198	185	96
14	0	0	1.682	227	190	102
15	0	0	0	251	199	112
16	0	0	0	263	201	115
17	0	0	0	260	200	115
18	0	0	0	259	202	114
19	0	0	0	263	202	115
20	0	0	0	265	200	114

using the sequential F test, lack-of-fit test, and other adequacy measures using the same software to obtain the best fit.

2.3 Desirability approach

There are many statistical techniques for solving multiple response problems like overlaying the contours plot for each response, constrained optimization problems, and desirability approach. The desirability method is preferred due to its simplicity and availability in the software and provides flexibility in weighting and giving importance for individual response. Solving such multiple response optimization problems by using this technique involves combining multiple responses into a dimensionless measure of performance called the overall desirability function. The desirability approach involves transforming each estimated response, Y_i , into a unitless utility bounded by $0 < d_i < 1$, where a higher d_i value

indicates that response value Y_i is more desirable, if $d_i=0$, which means a completely undesired response [16].

In this work, the individual desirability of each response, d_i , is calculated with Eqs. (3)–(6). The shape of the desirability function can be changed for each goal by the weight field. Weights are used to give more emphasis on the upper/lower bounds or to emphasize the target value. Weights can be ranged between 0.1 and 1; a weight greater than 1 gives more emphasis on the goal, while weights less than 1 give less emphasis. When the weight value is equal to 1, this will make the d_i vary from 0 to 1 in a linear mode. In the desirability objective function (D), each response can be assigned an importance (r), relative to other responses. Importance varies from the least important value of 1, indicated by (+), to the most important value of 5, indicated by (++++). If the varying degrees of importance are assigned to the different responses, the overall objective

function is shown in Eq. (7).

For goal of maximum, the desirability will be defined by

$$d_i = \begin{cases} 0, & Y_i \leq L_i \\ \left(\frac{Y_i - L_i}{H_i - L_i}\right)^w, & L_i < Y_i < H_i \\ 1, & Y_i \geq H_i \end{cases} \quad (3)$$

For goal of minimum, the desirability will be defined by

$$d_i = \begin{cases} 0, & Y_i \leq L_i \\ \left(\frac{H_i - Y_i}{H_i - L_i}\right)^w, & L_i < Y_i < H_i \\ 1, & Y_i \geq H_i \end{cases} \quad (4)$$

For goal as a target, the desirability will be defined by

$$d_i = \begin{cases} \left(\frac{Y_i - L_i}{T_i - L_i}\right)^{w_1}, & L_i < Y_i < T_i \\ \left(\frac{Y_i - H_i}{T_i - H_i}\right)^{w_2}, & T_i < Y_i < H_i \\ 0, & \text{Otherwise} \end{cases} \quad (5)$$

For goal within the range, the desirability will be defined by

$$d_i = \begin{cases} 1, & L_i < Y_i < H_i \\ 0, & \text{Otherwise} \end{cases} \quad (6)$$

$$D = \left(\prod_{i=1}^n d_i^{r_i} \right)^{1/\sum r_i} \quad (7)$$

where L is the low value, H is the high value, n is the number of responses in the measure and T_i is the target value of the i -th response [17].

2.4 Optimization

The optimization part in Design-Expert software V8 searches for a combination of factor levels that simultaneously satisfy the requirements placed (i.e., optimization criteria) on each of the responses and process factors (i.e., multiple-response optimization). Numerical and graphical optimization methods were used in this work by selecting the desired goals for each factor and response. As mentioned before, the numerical optimization process involves combining the goals into an overall desirability function (D). The numerical optimization feature in the design expert package finds

one point or more in the factors domain that will maximize this objective function. In a graphical optimization with multiple responses, the software defines regions where requirements simultaneously meet the proposed criteria. Also, superimposing or overlaying critical response contours can be defined on a contour plot. Then, a visual search for the best compromise becomes possible. In the case of dealing with many responses, it is recommended to run numerical optimization first; otherwise it is impossible to find out a feasible region. The graphical optimization displays the area of feasible response values in the factor space. Regions that do not fit the optimization criteria are shaded [17]. Figure 1 shows the flow chart of the optimization steps in the Design-Expert software.

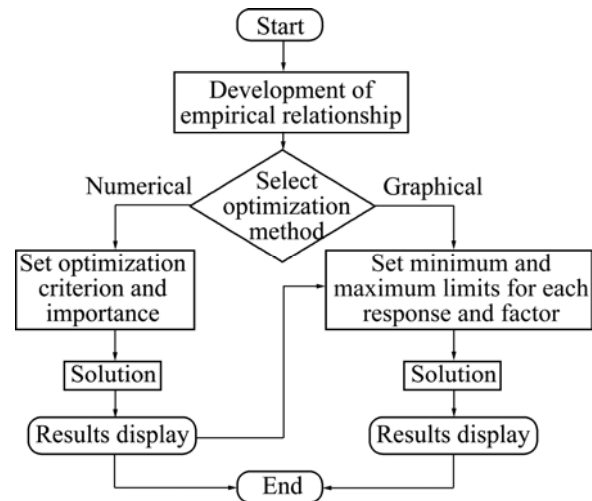


Fig. 1 Flow chart for optimization steps

3 Experimental work

Castings in size of 100 mm×100 mm×10 mm of unmodified AA6061 aluminium alloy matrix reinforced with 10% (volume fraction) of silicon carbide (SiC) particles were made by the stir casting method. These castings were hot rolled subsequently to reduce the thickness to 6 mm. Then they were machined to rectangular plates of 150 mm×100 mm×6 mm to carry out friction stir welding. The chemical composition and mechanical properties of the above plates were evaluated and presented in Tables 4 and 5, respectively. Square butt joint configuration was prepared to fabricate FSW joints. The initial joint configuration was obtained by securing the plates in position using mechanical clamps. The direction of welding was normal to the rolling direction. The joint dimensions are shown in Fig. 2(a). Single pass welding procedure was followed to fabricate the joints. Non-consumable tools made of high speed steel were used to fabricate the joints. The tool nomenclature is shown in Fig. 2(b). Based on three-factor five-level

central composite designs, as prescribed by the design matrix, twenty joints were fabricated. An indigenously designed and developed FSW machine (11 kW; 4000 r/min; 25 kN) was used to fabricate the joints. The welded joints were sliced using a power hacksaw and then machined to the required dimensions of tensile specimens, as shown in Figs. 2(c) and (d). The specimens were prepared as per the ASTM E8M-04 guidelines. Tensile test was carried out in 100 kN, servo controlled universal testing machine (FIE-BLUESTAR, UNITTEK94100) with a cross head speed of 0.5 mm/min at room temperature. The images of fabricated joints and tensile test specimens (before and after) are shown in Figs. 3(a) and (b), respectively. Vicker’s micro hardness testing machine (Shimadzu, HVM-2T) was employed for measuring the hardness of the weld nugget region with 0.5 N load at 15 s.

Table 4 Chemical composition of base aluminum alloy (mass fraction, %)

Al	Mg	Si	Cu	Cr	Fe	Mn	Ti	Zn
97.9	0.92	0.5	0.228	0.219	0.139	0.053	0.002	0.002

Table 5 Mechanical properties of cast AA6061/20%SiC_p MMC

Yield strength/MPa	Tensile strength/MPa	Elongation in 50 mm gauge length/%	Notch tensile strength/MPa	Hardness at 0.5 N (HV)
220	287	6.8	258	109

4 Developing empirical relationships

The fit summary tab in the Design-Expert software suggests the highest order of polynomial where the additional terms are significant and the model is not

aliased. The tensile strength (σ_b), notch tensile strength (σ_N) and hardness (H) of the weld nugget of FSW joints are functions of rotational speed (N), welding speed (S) and axial force (F) and can be expressed as

$$\sigma_b = f(N, S, F) \tag{8}$$

$$\sigma_N = f(N, S, F) \tag{9}$$

$$H = f(N, S, F) \tag{10}$$

And for the three factors, the selected polynomial could be expressed as

$$(\sigma_b) \text{ or } (\sigma_N) \text{ or } (H) =$$

$$b_0 + b_1(N) + b_2(S) + b_3(F) + b_{11}(N^2) + b_{22}(S^2) + b_{33}(F^2) + b_{12}(NS) + b_{13}(NF) + b_{23}(SF) \tag{11}$$

where b_0 is the average of responses and b_1, b_2, \dots, b_{33} are the coefficients that depend on respective main and interaction effects of the parameters. The value of the coefficient was calculated using the following expressions:

$$b_0 = 0.110749(\sum y) - 0.018738\sum(X_{ij}) \tag{12}$$

$$b_i = 0.023087\sum(X_{iy}) \tag{13}$$

$$b_{ij} = 0.0152625\sum(X_{ij}) + 0.001217\sum\sum(X_{ij}) - 0.018738(\sum y) \tag{14}$$

$$b_{ij} = 0.03125\sum(X_{ij})/n \tag{15}$$

All the coefficients were tested for their significance at 95% confidence level applying Fisher’s F test using Design-Expert V8 statistical software package. After determining the significant coefficients, the final models were developed using these coefficients only. The final empirical relationships to estimate tensile strength, notch tensile strength and hardness of weld nugget of FSW

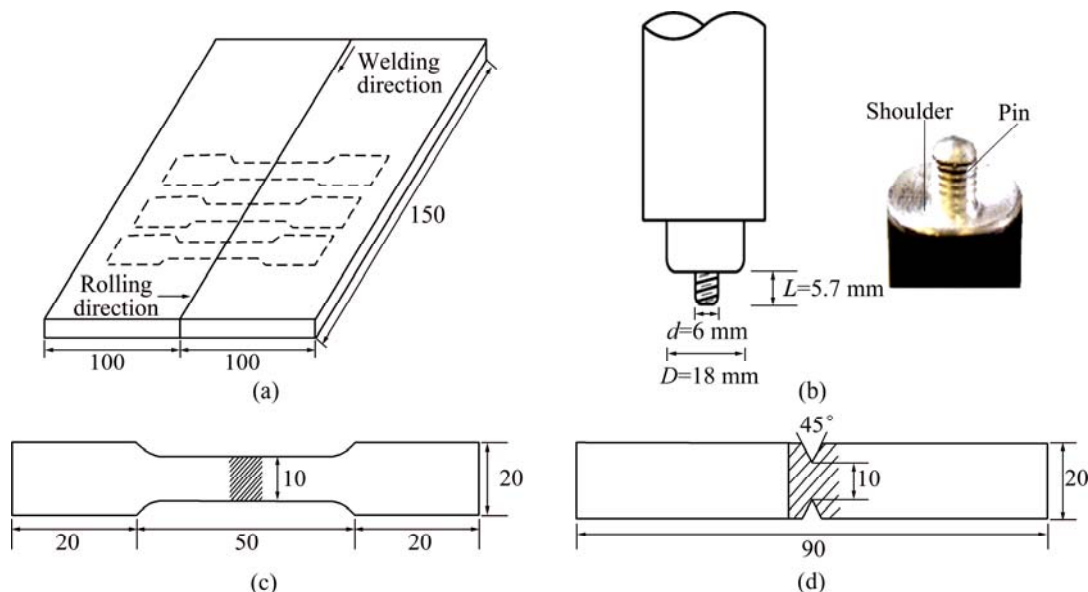
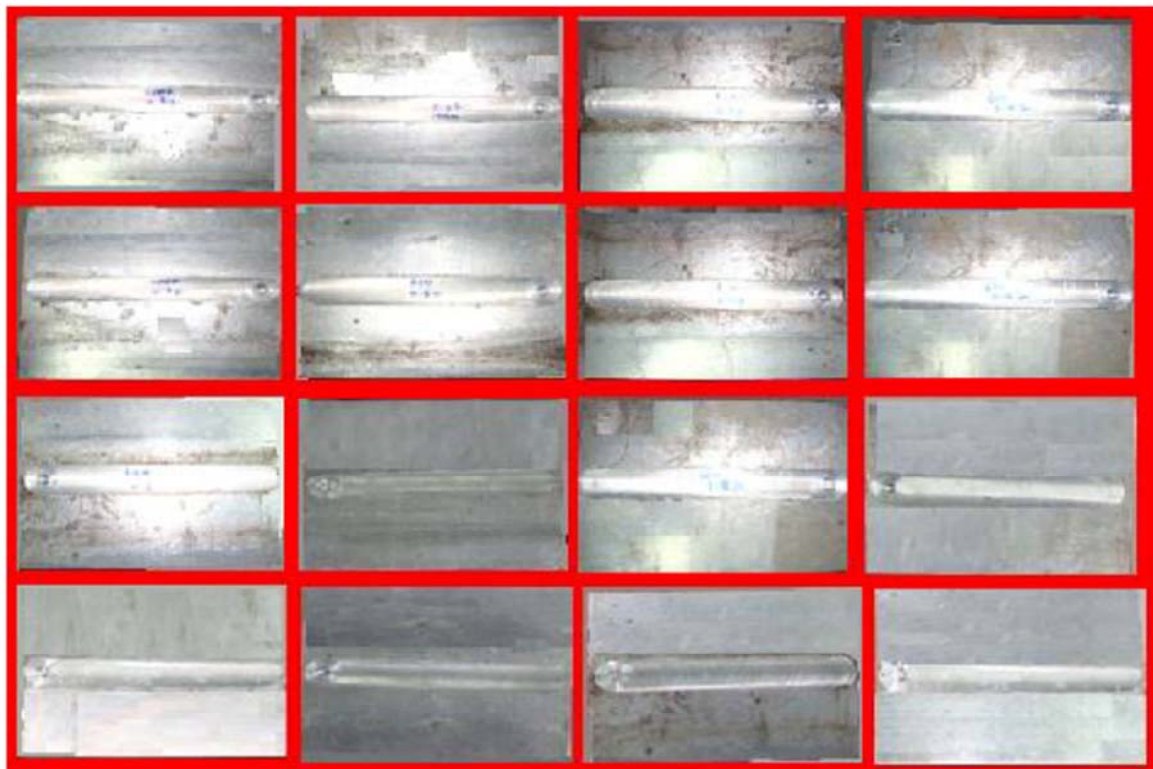


Fig. 2 Dimensions of joint (a); nomenclature of FSW tool (b); dimensions of un-notched tensile specimen (c) and notch tensile specimen (d) (Unit: mm)



(a)



(b)

Fig. 3 Fabricated joints (a) and tensile specimen (before and after testing) (b)

joints of cast AA6061/20%SiC_p MMCs, are given as

$$\sigma_b/\text{MPa}=260.33+19.99N+6.87S+5.62F+6.25NS+1.75NF+1SF-17.74N^2-19.16S^2-17.92F^2 \quad (16)$$

$$\sigma_N/\text{MPa}=200.753+4.826N+1.175S+1.275F-0.625NS+0.625NF-0.875SF-7.876N^2-7.7S^2-5.223F^2 \quad (17)$$

$$H/HV=114.206+1.690N+0.835S+1.398F-0.125NS+0.125NF-2.625SF-6.68N^2-5.8S^2-5.62F^2 \quad (18)$$

The adequacy of the developed empirical relationships was tested by the analysis of variance (ANOVA) technique [14]. Table 6 shows the ANOVA results of the tensile strength, notch tensile strength and weld nugget hardness, respectively. As per this technique, if the calculated value of the F-ratio of the developed model is less than the standard F ratio (from F table) value at a desired level of confidence (say 95%), then the model is said to be adequate within the confidence limit.

Table 6 ANOVA test results

Term	σ_b	σ_N	Hardness
First-order terms			
Sum of squares (SS)	6533.26	359.12	75.26
Degrees of freedom (df)	3	3	3
Mean squares (MS)	2177.75	119.71	25.09
Second-order terms			
Sum of squares (SS)	18939.34	2175.96	1453.24
Degrees of freedom (df)	9	9	9
Mean squares (MS)	2104.37	241.77	161.47
Error-order terms			
Sum of squares (SS)	124.83	7.333	6.833
Degrees of freedom (df)	5	5	5
Mean squares (MS)	24.96	1.466	1.366
Lack of fit			
Sum of squares (SS)	261.623	27.656	10.475
Degrees of freedom (df)	5	5	5
Mean squares (MS)	52.324	5.531	2.095
F ratio	1.25	1.25	1.25
Prob>F	54.45	69.09	93.289
R^2	0.980	0.984	0.988
R_{ratio} (calculated)	0.88608	0.89850	0.93923
R_{ratio} (from table)	1.2	1.2	1.2
12,5,0.05			
Model	Significant	Significant	Significant
F, Fisher's ratio			

5 Effect of process parameters on responses

In the following sections, whenever an interaction effect or a comparison between any two input parameters is being discussed, the other parameters are at center (middle) level.

5.1 Tensile strength

Perturbation plot shown in Fig. 4 illustrates the effect of the friction stir welding parameters on the tensile strength for an optimization design. This graph shows how the response changes as each factor moves from a chosen reference point, with all other factors held constant at the reference value [18]. A steep slope or curvature in a factor indicates that the response is sensitive to that factor. From the plot, it can be observed that the tool rotational speed is the most influential factor on tensile strength of the joint followed by axial force and then welding speed. Figures 5(a)–(c) are contour graphs showing the effect of the rotational speed and welding speed on the tensile strength, notch tensile strength and weld nugget hardness. When the rotational

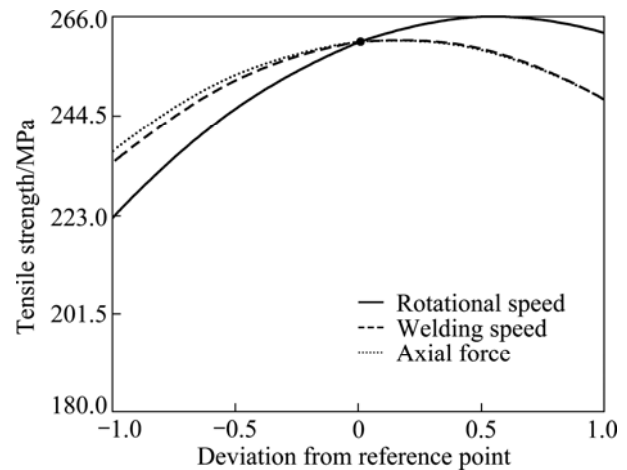


Fig. 4 Perturbation plot showing effect of FSW parameters on tensile strength of joint

speed is compared with the welding speed (at a constant axial force of 9 kN), the rotational speed is more sensitive to changes in tensile strength, as illustrated in Fig. 5(a). When the rotational speed is compared with the welding speed (at a constant axial force of 9 kN), the rotational speed is less sensitive to changes in notch tensile strength and weld nugget hardness. The interaction effect between the rotational speed and welding speed is more significant than the interaction effect between the other combinations of parameters. In FSW, the tool rotational speed is more sensitive than the other parameters. Especially, heat generation due to friction is mainly dependent on the tool rotational speed. The lower tool rotational speed produces less heat generation [19,20], irrespective of welding speed, subsequently the heat supplied to the base material is less, which causes insufficient material flow and less plasticization in stir zone and hence, the tensile strength is lower. The higher tool rotational speed produces high heat generation, irrespective of welding speed, subsequently the heat supplied to the base material is high, which causes turbulent material flow and grain coarsening in the stir zone and hence the tensile strength is lower. Neither low heat input nor high heat input is preferred in FSW, due to the reduction in tensile strength of the joints, as evident from Fig. 6. The dotted line or bandwidth shows the error in the tensile strength. The welding speed has a strong impact on productivity in streamlined production of friction stir welding of aluminium alloy sections. A significant increase in welding speed is achieved with high weld quality and excellent joint properties. The softened area is narrower for the higher welding speed than that for the lower welding speed. Thus, the tensile strength of welded aluminium alloy has a proportional relationship with welding speed [21]. Higher welding speeds are associated with low heat inputs, which results

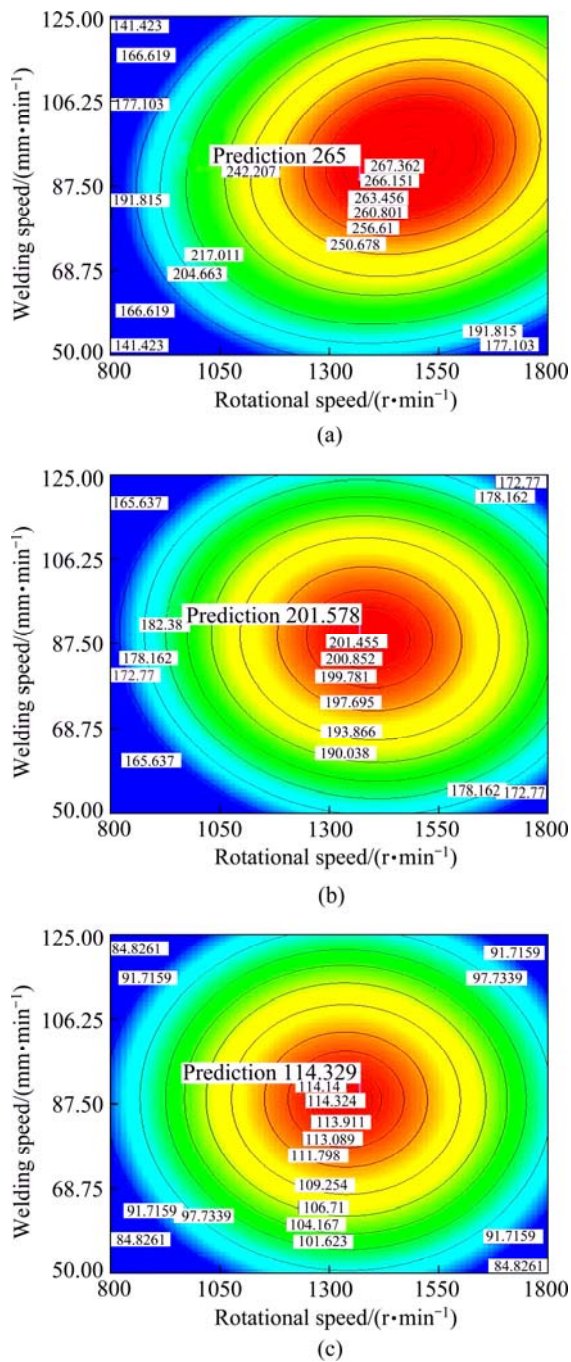


Fig. 5 Contour plots showing effect of rotational speed and welding speed on tensile strength, notch tensile strength and weld nugget hardness: (a) Tensile strength; (b) Notch tensile strength; (c) Weld nugget hardness

in faster cooling rates of the welded joint. This can significantly reduce the extent of metallurgical transformations taking place during welding (such as solubilisation, re-precipitation and coarsening of precipitates) and hence the local strength of individual regions across the weld zone [22]. When the welding speed is slower than a certain critical value, the FSW can produce defect-free joints. When the welding speed is faster than the critical value, welding defects can be

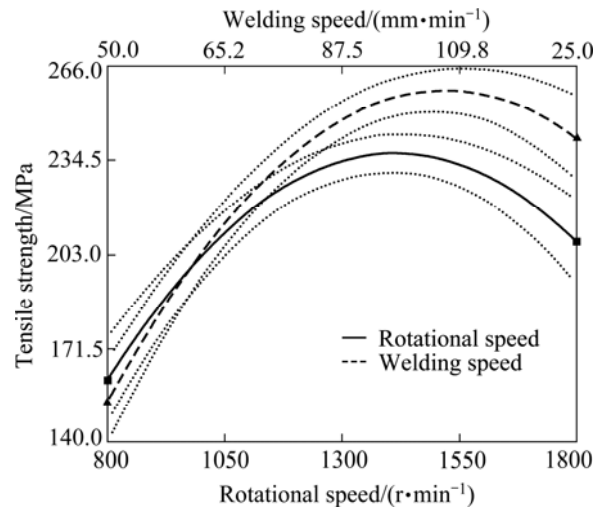


Fig. 6 Interaction effect between rotational speed and welding speed on tensile strength at $F=9$ kN

produced in the joints. The defects act as crack initiation sites during tensile test. Therefore, the tensile properties and fracture locations of the joints are determined by the welding speed [23].

5.2 Weld nugget hardness

Weld nugget hardness was measured at three different locations of mid-thickness region of the weld nugget and the average value was used for the analysis. The base metal records hardness of HV109, which is lower than that of stir zone. The weld nugget hardness is considerably higher than that of the base metal irrespective of the tool rotational speed used. There are two main reasons for improving hardness in the weld nugget. 1) The grain size of stir zone is much finer than that of base metal. The grain refinement plays an important role in material strengthening. According to the Hall-Petch equation, hardness increases as the grain size decreases. 2) The small intermetallic particles and uniformly distributed SiC_p improve the hardness, according to the Orowan hardening mechanism [24]. The difference of hardness between the heat affected zone and the stir zone is attributed to the grain refinement in the stir zone. Figure 7(a) shows that the lowest hardness is recorded in the joint fabricated with a tool rotational speed of 900 r/min at the HAZ region of retreating side. Retreating side (RS) records appreciably lower hardness values compared to advancing side (AS) irrespective of the tool rotational speed used. The joint fabricated with a tool rotational speed of 1500 r/min records the highest hardness value of HV114 in the weld nugget region. Similarly, the welding speed of 110 mm/min (Fig. 7(b)) and axial force of 11 kN (Fig. 7(c)) result in the maximum hardness compared to other process parameters, and this may be one of the reasons for superior strength properties of this joint.

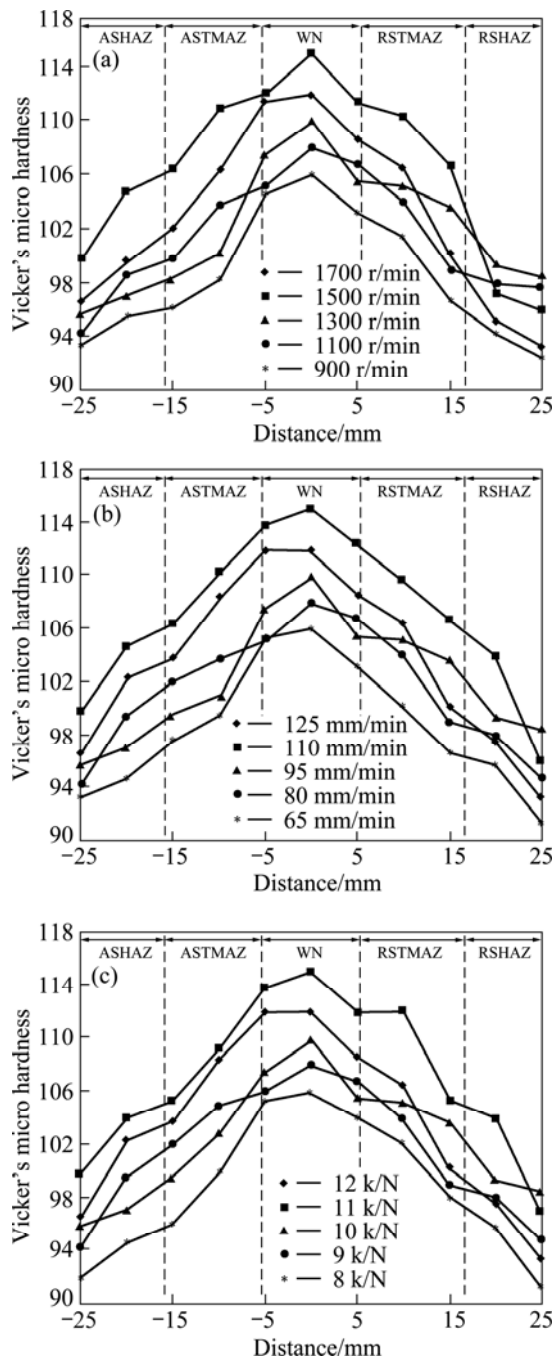


Fig. 6 Effect of process parameters on micro hardness of cast AA6061/20%SiC_p MMCs: (a) Tool rotational speed; (b) Welding speed; (c) Axial force

6 Optimization

The issue of linking between the strength and the hardness must be addressed as any increase in the strength is usually reflected in weld nugget hardness. As a consequence, both strength and hardness are usually studied together. On balance, and based on the above discussion, it is better to run an optimization study to find out the optimal welding conditions at which the desirable mechanical properties of the welded joint can be achieved. In fact, once the models have been developed and checked for adequacy, the optimization criteria can be set to find out the optimum welding conditions. In this work, two criteria were implemented to maximize the tensile strength, notch tensile strength and weld nugget hardness. The first criterion was to reach the maximum tensile strength, notch tensile strength and weld nugget hardness with no limitation on the welding parameters. While, in the second criterion the goal was to reach the maximum tensile strength, notch tensile strength and weld nugget hardness at relatively maximum rotational speed and welding speed. Table 7 summarizes these two criteria. While Tables 8 and 9 present the optimal solution based on the two optimization criteria determined by design-expert software. The optimization results clearly demonstrate that whatever the optimization criteria, the rotational speed has to be around its center limit of 1500 r/min to achieve the maximum tensile strength, notch tensile strength and weld nugget hardness. This result supports the discussion made earlier on the effect of rotational speed on the responses. Table 8 presents the optimal welding conditions according to the first criteria that would lead to the maximum tensile strength, notch tensile strength and weld nugget hardness of about 265 MPa, 201 MPa and HV114, respectively.

It is obvious that the graphical optimization allows visual selection of the optimum welding conditions according to certain criteria. The result of the graphical optimization is the overlay plots. These types of plots are

Table 7 Optimization criteria used in this work

Parameter or response	Limit		Importance	First criterion	Second criterion
	Lower	Upper			
Rotational speed/(r·min ⁻¹)	1002.698	1597.302	3	In range	Maximize
Welding speed/(mm·min ⁻¹)	65.2024	109.797	3	In range	Minimize
Axial force/kN	8.608	10.392	3	In range	In range
Ultimate tensile strength/MPa	150	265	5	Maximize	Maximize
Notch tensile strength/MPa	170	202	5	Maximize	Maximize
Hardness (HV)	90	115	5	Maximize	Maximize

Table 8 Optimal solution obtained by design-expert based on first criterion

Experiment No.	Input parameters			Output responses			Desirability
	Rotational speed/(r·min ⁻¹)	Welding speed/(mm·min ⁻¹)	Axial force/kN	UTS/MPa	NTS/MPa	Hardness (HV)	
1	1370.46	88.90	9.61	265.432	201.584	114.332	1
2	1300	87.5	9.5	265.120	201.241	114.031	1
3	1597.302	65.202	8.608	265.211	201.352	114.103	1
4	1002.698	65.202	10.391	265.263	201.252	114.212	1
5	1023.985	70.384	9.883	265.231	201.401	114.086	1
6	1220.383	83.517	9.686	265.032	201.302	114.237	1
7	1235.129	82.206	9.501	265.011	201.193	114.207	1
8	1039.028	97.123	9.123	265.250	201.202	114.230	1
9	1134.284	73.162	9.345	265.381	201.250	114.119	1
10	1256.653	95.081	9.855	265.301	201.158	114.257	1

Table 9 Optimal solution obtained by design-expert based on second criterion

Experiment No.	Input parameters			Output responses			Desirability
	Rotational speed/(r·min ⁻¹)	Welding speed/(mm·min ⁻¹)	Axial force/kN	UTS/MPa	NTS/MPa	Hardness (HV)	
1	1502.914	78.494	9.68	258.654	199.025	111.285	0.93212
2	1002.698	109.797	10.391	258.321	199.021	111.211	0.93201
3	1300	87.5	9.5	258.301	199.011	111.223	0.93213
4	1597.302	109.797	8.608	258.264	199.020	111.145	0.93214
5	1284.124	79.637	10.069	258.143	199.013	111.207	0.93215
6	1101.581	82.728	10.2889	258.062	199.014	111.218	0.93223
7	1431.11	77.252	10.363	258.208	199.012	111.177	0.93211
8	1130.954	89.390	9.630	258.513	199.015	111.107	0.93212
9	1403.639	92.503	8.804	258.305	199.016	111.117	0.93225
10	1047.83	70.116	9.995	258.403	199.010	111.203	0.93201

extremely practical for quick technical use in the workshop to choose the values of the welding parameters that would achieve certain response value for this type of material. The shaded areas on the overlay plots in Figs. 8 and 9 are the regions that meet the proposed criteria.

Table 8 and Figs. 8(a)–(c) show that the first criterion yields the maximum mechanical properties because the optimum welding parameters (tool rotational speed, welding speed and axial force) give the sufficient heat input to uniform flow of material, and the grains are finer in the stir zone. Similarly, Table 9 and Figs. 9(a)–(c) show that the second criterion yields the minimum mechanical properties because the maximum welding parameters (tool rotational speed, welding speed and axial force) give the excessive heat input to turbulent flow of material, and the grains are coarser in the stir zone.

6.1 Validation of developed relationships

To validate the developed models, three confirmation experiments were carried out with the welding conditions chosen randomly from the optimization results. For the actual responses, the average of three measured results was calculated. Table 10 summarizes the experimental condition, the average of actual experimental values, the predicted values, and the error. At the optimum values of process parameters, the average tensile strength of friction stir welded cast AA6061/20%SiC_p MMCs is found to be 265 MPa, which shows the excellent agreement with the predicted values. Microstructures of base material and weld nugget region of FSW joint fabricated using optimum parameters are shown in Fig. 10(a) and Fig. 11(a), respectively. Figure 11(a) reveal that there is no micron level defect due to sufficient heat generation and adequate

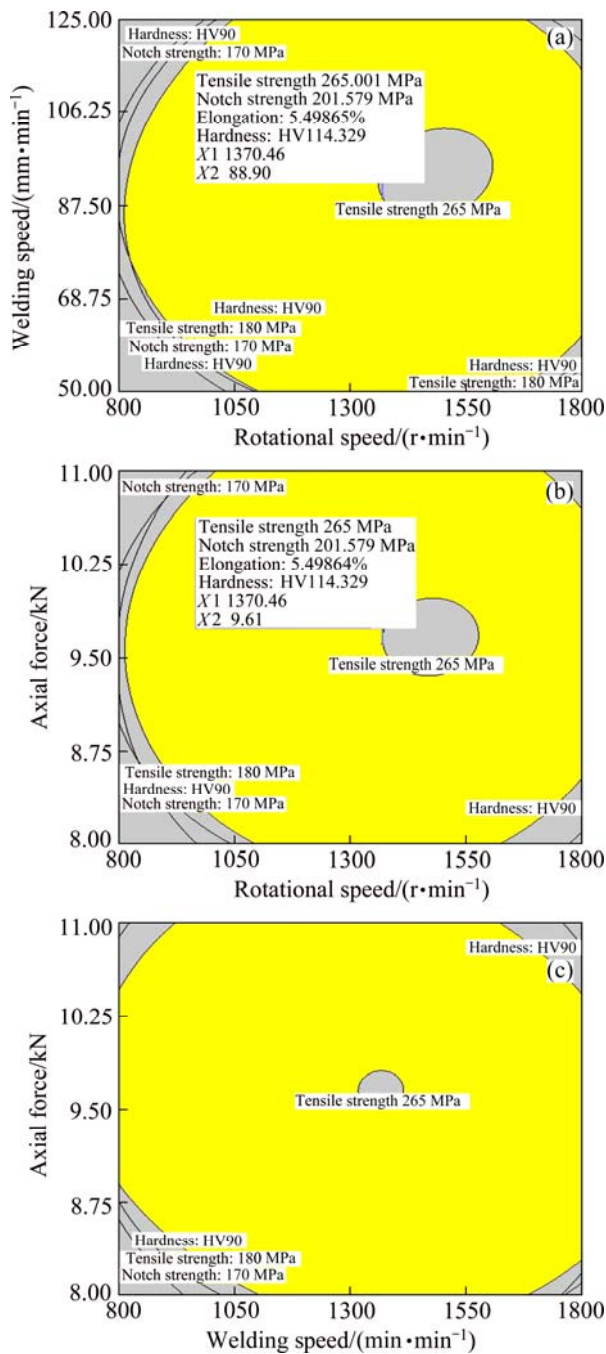


Fig. 8 Overlay plots showing region of optimal welding condition based on first criterion at $N=1370$ r/min, $S=88.9$ mm/min and $F=9.6$ kN

plastic flow of the material. Moreover, the grains are found to be finer than the base metal grains, as shown in Fig. 10(a).

Figures 10(b) and 11(b) show the SEM images indicating the size and distribution of SiC_p in the base metal and weld nugget region. It can be seen that finer SiC_p presents in the weld nugget region than in the base metal region.

The fracture surfaces of the tensile test specimens were characterized using SEM to understand the mode of

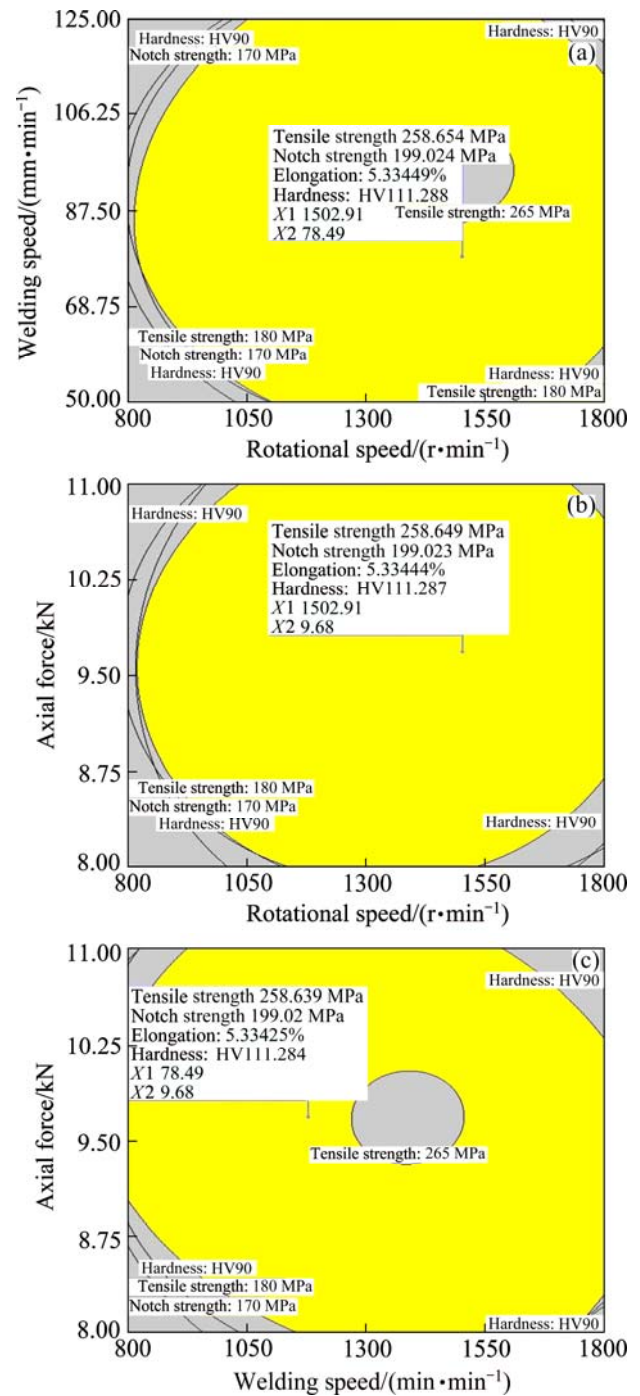
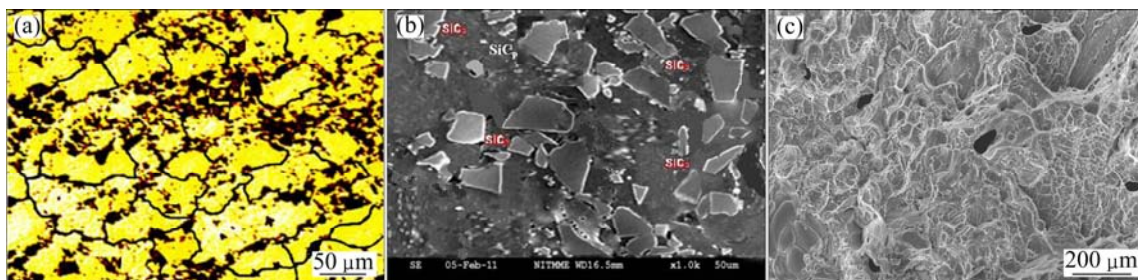
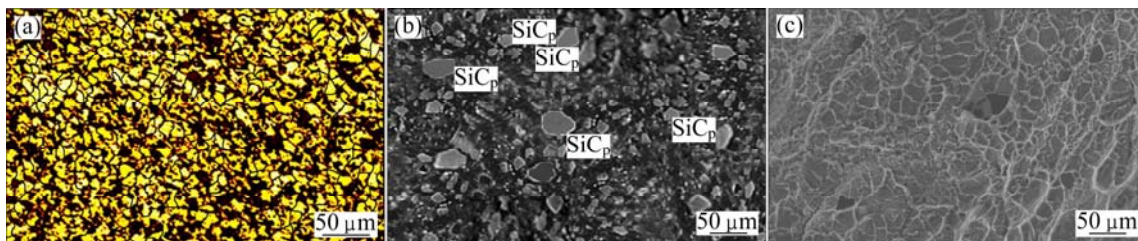


Fig. 9 Overlay plots showing region of optimal welding condition based on second criterion at $N=1502$ r/min, $S=78.5$ mm/min and $F=9.68$ kN

the failure. All the fracture surfaces invariably consist of dimples, which is an indication that most of the failure is the result of ductile fracture. The dimples on the fracture surface of the base metal are larger than those on the fracture surface of stir zone, as shown in Figs. 10(c) and 11(c). It is mainly due to the fact that the presence of hard and brittle SiC_p in the ductile Al matrix exerts constraints on the plastic flow of the matrix.

Table 10 Validation test results

Experiment No.	Input parameters			Responses								
				UTS			NTS			Hardness (HV)		
	Rotational speed/ ($\text{r}\cdot\text{min}^{-1}$)	Welding speed/ ($\text{mm}\cdot\text{min}^{-1}$)	Axial force/ kN	Actual/ MPa	Predicted/ MPa	Error/ %	Actual/ MPa	Predicted/ MPa	Error/ %	Actual	Predicted	Error/ %
1	1370.46	88.90	9.61	265	269	+1.48	201	206.68	+2.46	114	118.43	+3.46
2	1597.30	65.202	8.6	271	268.23	-1.03	212	208.42	-1.72	117	113.32	-3.24
3	1002.69	65.202	10.39	263	266.26	+1.22	198	192.34	-3.0	112	109.51	-2.3

**Fig. 10** Micrographs and fractographs of base material: (a) Optical micrograph; (b) SEM micrograph; (c) SEM fractograph**Fig. 11** Micrographs and fractographs of FSW joint fabricated using optimum parameters: (a) Optical micrograph; (b) SEM micrograph; (c) SEM fractograph

7 Conclusions

1) Multi-objective optimization using response surface methodology is an useful technique to optimize the friction stir welding parameters to obtain the maximum tensile strength and weld nugget of FSW joints.

2) A maximum ultimate tensile strength of 265 MPa, notch tensile strength of 201 MPa and hardness value of HV114.33 in the weld nugget region are exhibited by the FSW joints fabricated with the optimized welding parameters of rotational speed 1370 r/min, welding speed 88.9 mm/min and axial force 9.6 kN.

3) Rotational speed has greater influence on tensile strength, followed by axial force and welding speed.

Acknowledgements

The authors are grateful to the Center for Materials Joining and Research (CEMAJOR), Department of Manufacturing Engineering, Annamalai University,

Annamalai Nagar, India, for extending the facilities of metal joining and material testing to carry out this investigation.

References

- [1] PIRONDI A, COLLINI L, FERSINI D. Fracture and fatigue crack growth behavior of PMMC friction stir welded butt joints [J]. *Engineering Fracture Mechanics*, 2008, 75: 4333–4342.
- [2] THOMAS W M. Friction stir welding [P]. International Patent Application No. PCT/GB92/02203; GB Patent Application No. 9125978.8; U.S. Patent No. 51991460317.
- [3] DAWES C J. An introduction to friction stir welding and its development [J]. *Weld Material Fabrication*, 1995, 63: 2–16.
- [4] THOMAS W M, NICHOLAS E D. Friction stir welding for the transportation industries [J]. *Materials Design*, 1997, 18: 269–273.
- [5] VIJAYAN S. Multi objective optimization of friction stir welding process parameters on aluminum Alloy AA 5083 using Taguchi-based grey relation analysis [J]. *Materials and Manufacturing Processes*, 2010, 25, 1206–1212.
- [6] SARSILMAZ F. Statistical analysis on mechanical properties of friction-stir-welded AA1050/AA5083 couples [J]. *International Journal of Advanced Manufacturing Technology*, 2009, 43: 248–255.

- [7] TANSEL I N, DEMETGUL M, OKUYUCU H, YAPICI A. Optimizations of friction stir welding of aluminum alloy by using genetically optimized neural network [J]. *Int J Machine Tool Manufacture*, 2009, 44: 1205–1214.
- [8] RAJAKUMAR S, MURALIDHARAN C, BALASUBRAMANIAN V. Optimization of the FSW process and the tool parameters to attain a maximum tensile strength of AA7075-T6 aluminium alloy [J]. *J Eng Manuf*, 2010, 224: 1175–1191.
- [9] JAYARAMAN M, SIVASUBRAMANIAN R, BALASUBRAMANIAN V. Establishing relationship between the base metal properties and FSW process parameters of cast aluminium alloys [J]. *Material Design*, 2011, 31: 4567–4576.
- [10] LIM S, KIM S, LEE C G, KIM S. Tensile behavior of friction-stir-welded Al 6061-T651 [J]. *Metall Mater Trans A*, 2004, 35: 2829–2835.
- [11] ELANGOVA K, BALASUBRAMANIAN V. Influences of tool pin profile and tool shoulder diameter on the formation of friction stir processing zone in AA6061 aluminium alloy [J]. *Material Design* 2008, 293: 362–373.
- [12] BARCELLONA A, BUFFA G, FRATINI L, PALMERI D. On microstructural phenomena occurring in friction stir welding of aluminium alloys [J]. *J Mater Processing Technology*, 2006, 177: 340–343.
- [13] SATO Y S, TAKAUCHI H, PARK S H C, KOKAWA H. Characteristics of the kissing-bond in friction stir welded Al alloy 1050 [J]. *Mater Sci Eng A*, 2005, 405: 333–338.
- [14] MONTGOMERY D C. Design and analysis of experiments [J]. 2nd ed. New York: Wiley, 1984.
- [15] RAJAKUMAR S, MURALIDHARAN C, BALASUBRAMANIAN V. Establishing empirical relationships to predict grain size and tensile strength of friction stir welded AA 6061-T6 aluminium alloy joints [J]. *Transactions of Nonferrous Metals Society of China*, 2010, 20: 1863–1872.
- [16] MYERS R H, MONTGOMERY D C. Response surface methodology-process and product optimization using designed experiment [M]. London: Wiley, 1995.
- [17] Design-expert software v8 User's guide. Technical manual [M]. Minneapolis MN, Stat-Ease Inc, 2010.
- [18] ASTM E8 M-04 Standard test method for tension testing of metallic materials [M]. ASTM International, 2006.
- [19] SIVAKUMAR T, MANAVALAN R, MURALIDHARAN C. An improvement HPLC method with the aid of a chemometric protocol: Simultaneous analysis of Amlodipine and Atorvastatin in pharmaceutical formulations [J]. *J Sep Sci*, 2007, 30: 3143–3152.
- [20] RAJAKUMAR R, MURALIDHARAN C, BALASUBRAMANIAN V. Influence of friction-stir-welding process and tool parameters on strength properties of AA7075-T6 aluminium alloy joints [J]. *Material Design*, 2011, 32: 535–543.
- [21] WON BAE L E E. Mechanical properties related to microstructural variation of 6061 aluminium alloy joints by friction stir welding [J]. *Mater Trans*, 2004, 45(5): 1700–5.
- [22] LOMOLINO S, TOVO R, DOS SANTOS J. On the fatigue behavior and design curves of friction stir butt welded Al alloys [J]. *Int J Fatigue*, 2005, 27 : 305–16.
- [23] CHEN Ying-chun, LIU Hui-jie, FENG Ji-cai. Friction stir welding characteristics of different heat-treated-state 2219 aluminium alloy plates [J]. *Mater Science Eng A*, 2006, 420: 21–26.
- [24] WANG X H, WANG K S. Microstructure and properties of friction stir butt-welded AZ31 magnesium alloy [J]. *Mater Sci Eng A*, 2006, 431: 114–117.

Al/SiC_p 金属基复合材料 搅拌摩擦焊工艺参数的多目标优化

P. PERIYASAMY¹, B. MOHAN², V. BALASUBRAMANIAN³, S. RAJAKUMAR³, S. VENUGOPAL

1. Department of Mechanical Engineering, St. Peter's Engineering College, Avadi, Chennai 600 054, Tamil Nadu, India;

2. Department of Production Technology, MIT, Anna University, Chennai 600 044, Tamil Nadu, India;

3. Center for Materials Joining and Research (CEMAJOR), Department of Manufacturing Engineering, Annamalai University, Annamalinagar 608 002, Tamil Nadu, India;

4. IGCAR-Kalpakkam, Chennai, India

摘要: 碳化硅颗粒(SiC_p)增强铸造铝基复合材料(MMC)在制造高比强、高温性能好和耐磨的轻质结构件中得到广泛应用。焊接接头的性能取决于搅拌摩擦焊(FSW)的工艺参数。研究铸造 AA6061/20%SiC_p(体积分数)金属基复合材料焊接接头的抗拉强度、缺口拉伸强度和硬度,建立搅拌摩擦焊工艺参数(刀具转速、焊接速度和轴向力)与接头性能(抗拉强度、缺口拉伸强度和焊点硬度)之间的关系,确定最佳的焊接条件,以最大限度地提高接头的力学性能。结果表明,当搅拌针转速为 1370 r/min、焊接速度为 88.9 mm/min 和轴向力为 9.6 kN 时,接头的最大抗拉强度、缺口拉伸强度和硬度分别为 265 MPa、201 MPa 和 HV114。

关键词: 金属基复合材料; 焊接; 显微组织

(Edited by Sai-qian YUAN)